Reprinted from JOURNAL OF APPLIED PHYSICS, Vol. 36, No. 6, 1803–1807, June 1965

X-Ray Topography of Decorated Dislocations in Magnesium Oxide*

A. R. LANG
H. H. Wills Physics Laboratory, University of Bristol, England
AND
G. D. MILES
Metallurgy Division, Atomic Energy Research Establishment, Harwell, England
(Received 6 January 1965)

Combined x-ray topographic and ultramicroscopic studies have shown a one-to-one correspondence between dislocation lines and chains of submicroscopic light-scattering bodies within a magnesium oxide crystal in the "as-received" state. Dislocations with any orientation and Burgers' vector were found to be decorated. The geometry and Burgers' vectors of various unusual dislocation configurations have been determined. These special configurations all arose from the extension of edge segments in the course of intense dislocation climb combined with a strong preference for a line orientation parallel to a cube direction. The relationship of such configurations to the general distribution of dislocations showed that the epoch of intense dislocation climb had occurred late in the evolution of the dislocation distribution. X-ray diffraction evidence on whether the climb was due to the absorption of interstitials or of vacancies is as yet inconclusive.

I. INTRODUCTION

A RELATIVELY rare but quite remarkable type of dislocation configuration in single crystals of magnesium oxide has been investigated. It was discovered through ultramicroscopic observations because the dislocations concerned are decorated by submicroscopic precipitates which, under high magnification, appear visually as bright light-scattering points upon a dark background.[1]

The scope of the x-ray topographic investigation encompassed observations to check the association between dislocations and lines of precipitates, to determine the Burgers' vectors of the characteristic elements of this special dislocation distribution, and to study the over-all lattice perfection and dislocation visibility in relation to the concentration of light-scattering bodies present. As a background to the investigation, the information obtained in previous x-ray topographic examinations of magnesium oxide could be drawn upon,[2,3] and observations that had been made on a variety of lithium fluoride specimens proved relevant. Thus assisted, it was possible to decipher some of the history of development of the special dislocation configuration, but the origin of the atomic rearrangements producing it is still unexplained.

II. EXPERIMENTAL METHODS

The dislocation configurations of present interest have been detected by light scattering in 5 out of 25 crystals obtained from Semi-Elements, Inc., Saxonburg, Pennsylvania, and in 1 out of 35 obtained from the Norton Company, Worcester, Massachusetts. The crystals were in all cases in the "as-received" state. The x-ray experiments were carried out on one of the Semi-Elements crystals. A plate about 1 cm square and $\frac{1}{4}$ mm in thickness was cleaved from a block and then etched in hot orthophosphoric acid until part of it was reduced to a thickness of about 50 μ. X-ray projection topographs[4] were taken with x rays transmitted through the specimen. Figure 1 is a stereographic projection on the plane of the specimen. Bragg reflections were obtained from all planes whose normals are indicated in Fig. 1, except from the specimen plane itself (001). The direction [001] is taken as pointing from the x-ray source towards the observer. All the topographs reproduced here except Fig. 4 are shown in the orientation of Fig. 1, and they were all taken with Cu $K\alpha_1$ radiation. The four stereo pairs of reflections (i.e., 200, $\bar{2}00$; 020, $0\bar{2}0$; 220, $\bar{2}\bar{2}0$; and $2\bar{2}0$, $\bar{2}20$) enabled the spatial distribution of dislocations and low-angle boundaries within the depth of the specimen to be found.[5]

After the complete set of topographs had been taken, certain regions were photographed with the ultramicroscope, using the technique described by Miles.[1] A slight etching was needed to remove some surface opacity and this resulted in the loss of a few dislocation features lying close to the surfaces. Following the ultramicroscopic examination the specimen was re-etched and topographs were again taken from all the planes [except (001)] indexed on Fig. 1. Specimen thickness in the regions studied x-ray topographically can be

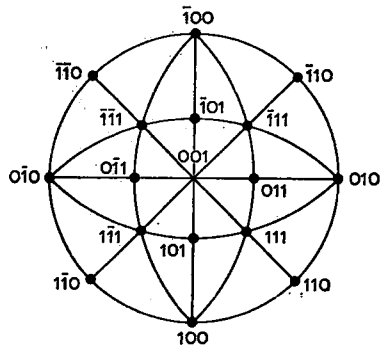

FIG. 1. Stereographic projection on plane of specimen.

* Research supported in part by the Aerospace Research Laboratories, O.A.R., through the European Office of Aerospace Research, United States Air Force.

[1] G. D. Miles, J. Appl. Phys. 36, 1471 (1965).
[2] V. F. Miuscov and A. R. Lang, Kristallografiya 8, 652 (1963).
[3] A. R. Lang and V. F. Miuscov, Phil. Mag. 10, 263 (1964).
[4] A. R. Lang, Acta Cryst. 12, 249 (1959).
[5] A. R. Lang, J. Appl. Phys. 30, 1748 (1959).

FIG. 2. Mosaic of ultramicrographs (a) and x-ray topographs of same area: (b) $0\bar{2}0$ reflection, (c) $\bar{2}00$ reflection, scale mark 50 μ. Specimen thickness about 50 μ.

measured to within a few microns by the order of the Pendellösung fringes[6] (i.e., equal-thickness fringes).

[6] N. Kato and A. R. Lang, Acta Cryst. 12, 787 (1959).

III. OBSERVATIONS

A. The General Arrangement of Dislocations

The x-ray topographs exhibit features of interest on two size scales. First, on the millimeter scale, we can survey the network of low-angle boundaries separating the subgrains and perceive the gross pattern of dislocations within subgrains. We find in all subgrains a pronounced anisotropy of distribution of Burgers' vectors among their possible directions. Second, on a finer scale, ranging from 100 μ down to the limit of resolution of adjacent dislocations (about 2–3 μ), we encounter the unusual configurations of individual dislocations which render this specimen remarkable. All of them appear to have arisen through the process of dislocation climb, which has been active to a marked degree, and has caused a great increase in total dislocation-line length through the growth of edge segments. Such edge segments, moreover, have a strongly preferred orientation, that of a cube direction.

Figure 2(a) is a mosaic of light-scattering micrographs, covering an area of 0.45 mm^2. In this field most of the special configurations are in evidence. Typical individual elements which make up the pattern have been shown at higher magnification elsewhere.[1] Figure 3 contains sketches (not all on the same scale) of the basic elements as they appear when looking perpendicularly at the specimen in the orientation of Fig. 1. The distorted helices in Fig. 3(a) have major diameters ranging from 20–200 μ. Another basic element is the line with "spikes" pulled out on one side of it, as in Fig. 3(b). The spike axis lies parallel to a cube direction. Some examples of this feature are apparent in Figs. 2(c) and 5(b) within the subgrains and numerous spikes are seen protruding from low-angle boundaries. A group of spikes in Fig. 2(c) is indicated by an arrow. A more complicated feature is the "Christmas tree," Fig. 3(c), a dendritic formation consisting of a "stem" or "axis" lying generally in a ⟨110⟩ direction with "branches" in the form of miniature spikes lying in a cube direction normal to the stem. Trees rarely exceed 50 μ in projected height and they are more frequently about $\frac{1}{2}$ or $\frac{1}{3}$ of this size. The details of the structure are not generally resolved on the x-ray topographs. Thus, trees usually appear simply as triangular patches of darkening, and they can be recognized in this guise in Fig. 2, (b) and (c); see, for example, the image in Fig. 2(c) of the two superimposed trees situated near the right-hand margin of Fig. 2(a) and indicated by the arrow (1). The stem and branches of larger trees can sometimes be distinguished. Their resolution was just achieved in the case of the double tree shown in the stereo pair of topographs, Fig. 4, (a) and (b).

A further characteristic feature is the elongated loop (not drawn in Fig. 3). Such loops appear in profusion in Figs. 2(b) and 5(a) as well as in the optical micrographs in Fig. 2(a).

Since we are here particularly concerned with the smaller-scale features of the dislocation pattern, we show only selected small parts of the x-ray topographs, reproduced at relatively high magnification (by x-ray topographic standards). The area covered by each topograph covers less than the average cross section of a subgrain, but in each field some subgrain boundaries can be seen. They appear as dark bands with a width that depends simply upon the angle the boundary surface makes with the diffracted x-ray beam at a given specimen thickness. The x-ray topographs show clearly the relationship of the special configurations (such as those drawn in Fig. 3) to the gross features of the dislocation distribution. It is found that in any region the frequency of occurrence of the various elements drawn in Fig. 3 depends upon the predominant Burgers' vector and type (i.e., mainly edge or mainly screw) of the general dislocation population, and is thus related to the anisotropy of distribution of Burgers' vectors already mentioned. This relationship becomes more readily apparent by comparing x-ray topographs of different reflections than by inspection of the light-scattering micrographs which show all decorated dislocations simultaneously. The anisotropy of distribution of Burgers' vectors in this specimen is shown most strikingly by the different density of dislocations visible in reflections from the (100) and (010) planes. Compare, for example, Fig. 2(b) with 2(c), and Fig. 5(a) with 5(b). In the 200 or $\bar{2}00$ reflections the images of dislocations having Burgers' vectors parallel to $[0\bar{1}1]$ or $[011]$ are suppressed, and in the 020 or $0\bar{2}0$ reflections the weak or missing lines have Burgers' vectors parallel to $[101]$ or $[\bar{1}01]$. The dominance of Burgers' vector parallel to $[0\bar{1}1]$ or $[011]$ is apparent; a study of other reflections shows that Burgers' vectors parallel to $[0\bar{1}1]$ are more numerous than those parallel to $[011]$. Quite surprising is the rarity of Burgers' vectors parallel to $[110]$ or $[1\bar{1}0]$: such dislocations would be equally visible in the $\bar{2}00$ and $0\bar{2}0$ reflections. In fact, inspection of the topograph pairs in Fig. 2, (b) and (c), or Fig. 5, (a) and (b), shows only a few dislocation features common to both members of the pair. These features lie generally in the $[110]$ or $[1\bar{1}0]$ direction.

No evidence has been accumulated to suggest that dislocations seen well-resolved on the topographs have Burgers' vectors other than those expected in the rock-salt structure, i.e., $\frac{1}{2}\langle 110\rangle$. It follows that a pair of topographs, such as the 200 and 020 reflections, will together show the total dislocation population, and the sum of their dislocation images can be compared with the light-scattering pattern. After making due allowance for parallax effects and for the loss of a few features near the surface between taking the x-ray topographs and the ultramicrographs, it is readily apparent that the x-ray and optical patterns agree completely. This agreement can be seen, for example, by comparing Figs. 2(a), 2(b), and 2(c). Thus, at a certain stage in the history of the specimen, *all* dislocations became decorated, and *no* detectable movement of dislocations relative to the precipitates has occurred subsequently.

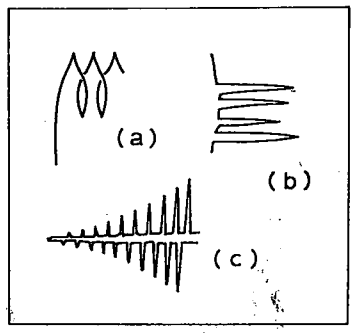

FIG. 3. Elements of dislocation configuration as they appear looking along $[001]$: (a) helix, (b) line with spikes, (c) Christmas tree.

B. Loops, Helices, and Spikes

The great majority of the dislocations visible within the subgrains in the 020 and $0\bar{2}0$ topographs have the form of loops and helices. In the 200 and $\bar{2}00$ topographs, on the other hand, recognizable loops and helices are extremely rare; none can be seen, for example, in the parts of the $\bar{2}00$ topograph reproduced in Figs. 2(c) and 5(b). All loops appearing in the 020 and $0\bar{2}0$ topographs are highly elliptical with their major axis lying along $[100]$, and the turns of the helices exhibit varying degrees of a similar ellipticity. In addition, the loops and helices often possess cusps at the ends of their major diameters, after the fashion shown in Fig. 3(a). Loops whose long axes lie along $[100]$ have Burgers' vectors parallel to $[011]$ or $[0\bar{1}1]$. The mean directions of axes of helices are found to be those of the Burgers' vector of the helix ($[0\bar{1}1]$ for the majority), but with a scatter of up to $\pm 20°$ from the Burgers' vector direction. In favorable cases the helix directions can be determined to within $\pm 3°$. When the turns of a helix are closely spaced, the varying degree of superimposition of images of the turns in different reflections renders it difficult to assess relative image visibility. However, if the helix has a "tail" of pure edge dislocation attached to it, as have, for example, the rather tight helices seen to the left of the low-angle boundary node in Fig. 5(a), then the Burgers' vector identification can be made

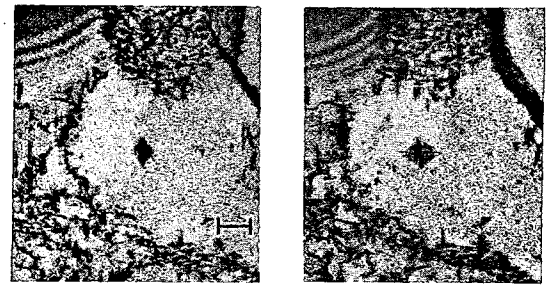

(a) (b)

FIG. 4. Stereo pair showing orientation of trees; direction $[100]$ is horizontal: (a) $\bar{2}00$ reflection, left-eye view, (b) 200 reflection, right-eye view, scale mark 50 μ. Specimen thickness about 90 μ.

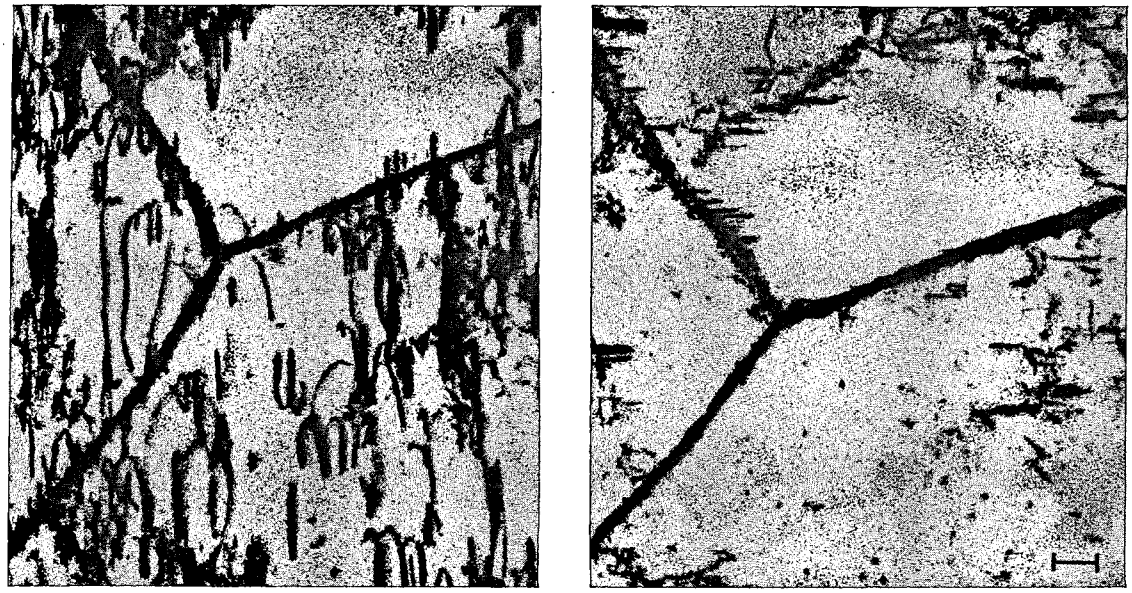

(a) (b)

FIG. 5. Field including a low-angle boundary node: (a) $0\bar{2}0$ reflection, (b) $\bar{2}00$ reflection, scale mark 50 μ. Specimen thickness about 50 μ.

upon this edge segment without difficulty. It is observed that the majority of helices having a given Burgers' vector have the same sense (i.e., most helices with Burgers' vector parallel to [011] are left-handed screws, and most with Burgers' vector parallel to $[0\bar{1}1]$ are right-handed screws). This observation tells us that the majority of *Burgers' vectors* in a given direction have the same sense, since all helices are likely to have developed in the same way, whether it be by absorption of vacancies or of interstitials. (How the hand of a helix formed by climb is related to the sense of its Burgers' vector has been explained by Dash.[7]) Under suitable diffraction conditions x-ray topographs can show the sense as well as the direction of dislocations having an edge component.[8] Unfortunately, diffraction evidence for the sense of Burgers' vectors of helices and of the edge-dislocation tails attached to some of them was very inconclusive in the experiments here described.

The great difference in appearance between topographs taken with reflections from (100) and from (010) planes arises not only from the much sparser density of lines in the former topographs but also from the replacement of loops and helices by the line-with-spikes as the typical element of the pattern. The spikes appear in the orientation sketched in Fig. 3(b), i.e., parallel to [010]. Such spikes have Burgers' vectors along [101] or $[\bar{1}01]$. Segments of a line-with-spikes often lie close to the (001) plane. It should be pointed out that there is no sharp division between the configurations of Fig. 3(a) and 3(b). Transitional forms are found in both 200 and 020 topographs. It appears that it was the original orientation of the dislocation that decided whether it took the shape of Fig. 3(a) or 3(b) after climb. Dislocations that were mainly screw turned themselves into helices. It appears that production of spikes parallel to [010] was favored if the original line orientation was not far from [100], or at least made only a small angle with the plane (010).

C. Trees

Certain typical features of the "Christmas tree" phenomenon are illustrated in the stereo pair, Fig. 4, (a) and (b). In the center of the field, where the specimen thickness is about 90 μ, a pair of opposed trees is seen. They both lie within about 3° of the (101) plane, according to measurements of the topographs. The tree stems lie parallel to $[\bar{1}01]$ and the branches parallel to [010], stem and branches being just resolvable on the original topograph plates. The height of each tree is about 30 μ. Very typical features to note are, first, that the trees lie in or close to a {110} plane; second, that they appear at a point relatively remote from other dislocations; and, third, that they spring from a root where there is some further unresolved structure. These trees are invisible in the 020 and $0\bar{2}0$ reflections. In fact, trees are always invisible in the reflection from the plane normal to their side branches. Thus the two superimposed trees with branches parallel to [010] indicated by the arrow (1) in Fig. 2(a) are strongly visible in the $\bar{2}00$ reflection, 2(c), but are invisible in the $0\bar{2}0$ reflection, 2(b). On the other hand, the tree located about 60 μ to the left of the trees arrowed, which has its stem roughly parallel to $[0\bar{1}1]$ and branches parallel to [100], is clearly visible in Fig. 2(b)

[7] W. C. Dash, J. Appl. Phys. 31, 2275 (1960).
[8] M. Hart and A. R. Lang, Acta Cryst. 16, A102 (1963).